Since January 2020 Elsevier has created a COVID-19 resource centre with free information in English and Mandarin on the novel coronavirus COVID-19. The COVID-19 resource centre is hosted on Elsevier Connect, the company's public news and information website.

Virology 566 (2022) 60–68

Contents lists available at ScienceDirect

Virology

journal homepage: www.elsevier.com/locate/virology

Pharmacologic profiling reveals lapatinib as a novel antiviral against SARS-CoV-2 in vitro

M.H. Raymonda [a,d,1], J.H. Ciesla [a,d,1], M. Monaghan [a,d,1], J. Leach [b], G. Asantewaa [a,c,d], L. A. Smorodintsev-Schiller [c,d], M.M. Lutz IV [b], X.L. Schafer [a,d], T. Takimoto [b], S. Dewhurst [b], J. Munger [a,b,d,*], I.S. Harris [c,d,**]

[a] Department of Biochemistry and Biophysics, School of Medicine and Dentistry, University of Rochester, Rochester, NY, USA
[b] Department of Microbiology and Immunology, University of Rochester, Rochester, NY, USA
[c] Department of Biomedical Genetics, University of Rochester Medical Center, Rochester, NY, USA
[d] Wilmot Cancer Institute, University of Rochester Medical Center, Rochester, NY, USA

ARTICLE INFO

Keywords:
Lapatinib
OC43
SARS-CoV-2
Pharmacologic screening
Coronavirus
Betacoronavirus

ABSTRACT

The emergence of SARS-CoV-2 virus has resulted in a worldwide pandemic, but effective antiviral therapies are not widely available. To improve treatment options, we conducted a high-throughput screen to uncover compounds that block SARS-CoV-2 infection. A minimally pathogenic human betacoronavirus (OC43) was used to infect physiologically-relevant human pulmonary fibroblasts (MRC5) to facilitate rapid antiviral discovery in a preclinical model. Comprehensive profiling was conducted on more than 600 compounds, with each compound arrayed across 10 dose points. Our screening revealed several FDA-approved agents that can attenuate both OC43 and SARS-CoV-2 viral replication, including lapatinib, doramapimod, and 17-AAG. Importantly, lapatinib inhibited SARS-CoV-2 RNA replication by over 50,000-fold. Further, both lapatinib and doramapimod could be combined with remdesivir to improve antiviral activity in cells. These findings reveal novel therapeutic avenues that could limit SARS-CoV-2 infection.

1. Introduction

In 2020, from February to late November, the COVID-19/SARS-CoV-2 pandemic killed over 256,000 people in the United States (CDC data tracker) and over 1,368,000 people globally (WHO Operational Update). Currently, effective treatments to inhibit SARS-CoV-2 morbidity and mortality are not available, and as such, the pandemic is predicted to continue to take a devastating toll on both human health and economic activity.

Since the pandemic began, there has been a strong interest in screening existing compound libraries for their ability to inhibit SARS-CoV-2 replication. Traditionally, high-throughput antiviral screens test compounds in a host cell line that can be efficiently infected by the virus and is capable of supporting high-titer viral replication (Bojkova et al., 2020; Gordon et al., 2020). Many times, this results in the host cell type being derived from a non-physiological source, e.g., from a different species (monkey), tissue (kidney), or genetic background (tumors) than what is important for human infection and the associated pathology. This has been the case for many SARS-CoV-2 screens, which have relied on monkey kidney cells, e.g., Vero cells, to identify potential SARS-CoV-2 antiviral agents (Bojkova et al., 2020; Gordon et al., 2020). Further, recent findings suggest these models are insufficient to identify effective SARS-CoV-2 antivirals in human cells (Dittmar et al., 2021). In addition, many screening efforts have focused on screening libraries that contain compounds at a single high concentration, e.g., 5 or 10 μM (Riva et al., 2020). While this is useful for drug discovery efforts using biochemical assays, these libraries are poorly suited for more complicated screens with live cells, as high drug concentrations can potentially reduce cell viability and induce off-target effects. Screening at only a single high dose, therefore, may completely miss many compounds that may be effective in limiting viral replication at lower concentrations.

To address these issues, we developed an anti-coronaviral screening

* Corresponding author. Department of Biochemistry and Biophysics, School of Medicine and Dentistry, University of Rochester, Rochester, NY, USA.
** Corresponding author. Department of Biomedical Genetics, University of Rochester Medical Center, Rochester, NY, USA.
E-mail addresses: joshua_munger@urmc.rochester.edu (J. Munger), isaac_harris@urmc.rochester.edu (I.S. Harris).
[1] Authors contributed equally to this work.

https://doi.org/10.1016/j.virol.2021.11.008
Received 27 July 2021; Received in revised form 18 November 2021; Accepted 19 November 2021
Available online 27 November 2021

platform in which physiologically-relevant non-transformed human pulmonary fibroblasts infected with coronavirus were tested against compounds across a wide range of doses (20 μM to 1 nM). This enabled us to identify concentrations of compounds that inhibit virally-induced killing while also maintaining cell viability. Similar drug screening approaches have successfully identified selective vulnerabilities in cancer cells (Harris et al., 2019; Nicholson et al., 2019; Shu et al., 2020). To facilitate rapid screening, we tested the minimally pathogenic human coronavirus, OC43, which belongs to the same betacoronavirus genus as SARS-CoV-2. We then examined the ability of the compound hits from our high-throughput screen to inhibit SARS-CoV-2 infection. This approach selects for antiviral compounds that may exhibit broad activity towards coronaviruses. We have identified and validated several compounds that inhibit the replication of OC43 and SARS-CoV-2. Of particular note, we find that lapatinib, an FDA-approved drug that exhibits a good toxicity profile in humans (Spector et al., 2015), inhibits SARS-CoV-2 RNA replication by over 50,000-fold.

2. Results

2.1. High-throughput screening reveals compounds with novel activity against coronaviruses

Since a BSL3 high-throughput screening facility was not readily available, compounds were screened against the virus OC43, a minimally pathogenic human betacoronavirus of the same coronavirus genus as SARS-CoV-2. We tested whether OC43 would replicate in MRC5-hT cells (herein referred to as MRC5 cells), which are human pulmonary fibroblasts (immortalized with human TERT) that have previously been shown to be an effective model of viral infection into non-transformed cells (Rodriguez-Sanchez et al., 2019). The OC43 virus rapidly replicated in MRC5 cells as indicated by increased viral RNA and protein abundance in cells upon infection (Figs. S1A and S1B). Viral replication causes cell death, known as the cytopathic effect (CPE). As a readout of the ability of a compound to block viral replication, inhibition of CPE was quantified using an image-based readout. OC43 induced substantial CPE in MRC5 cells (Fig. 1A), and conditions were optimized to generate a robust Z' factor for the screen (Zhang et al., 1999) (Z' = 0.66) (Fig. S2). To comprehensively understand the pharmacologic profile for each compound, a new platform was developed, termed the Multifunctional Approach to Pharmacologic Screening (MAPS) (Fig. 1B). Here, each drug in our compound library was arrayed across 10 dose points, ranging from 20 μM to 1 nM. These multiple concentrations provided a broad picture of each drugs' ability to block virus-induced CPE. For our screen, we repurposed a drug library that focused on cancer and metabolic targets, which previously had been used to examine drug sensitivities in cancer cells (Harris et al., 2019; Nicholson et al., 2019; Shu et al., 2020). The maximal inhibition of viral killing in cells (at any dose) was used to identify compounds as potential hits (Fig. 1C, Table S1). Drugs spanning a wide range of target proteins were identified as antivirals (Fig. 1D). Three of the top-scoring compounds were doramapimod (BIRB 796), lapatinib, and 17-AAG. Doramapimod is a pan-inhibitor of p38 MAPKs (Pargellis et al., 2002), lapatinib is a dual inhibitor of EGFR/HER2 (Burris et al., 2005), and 17-AAG blocks HSP90 activity (Kamal et al., 2003). Upon validation using a larger number of drug concentrations, the hit compounds demonstrated robust inhibition of CPE (Fig. 1E). Interestingly, some compounds, such as 17-AAG, demonstrated that screening at μM concentrations precluded the

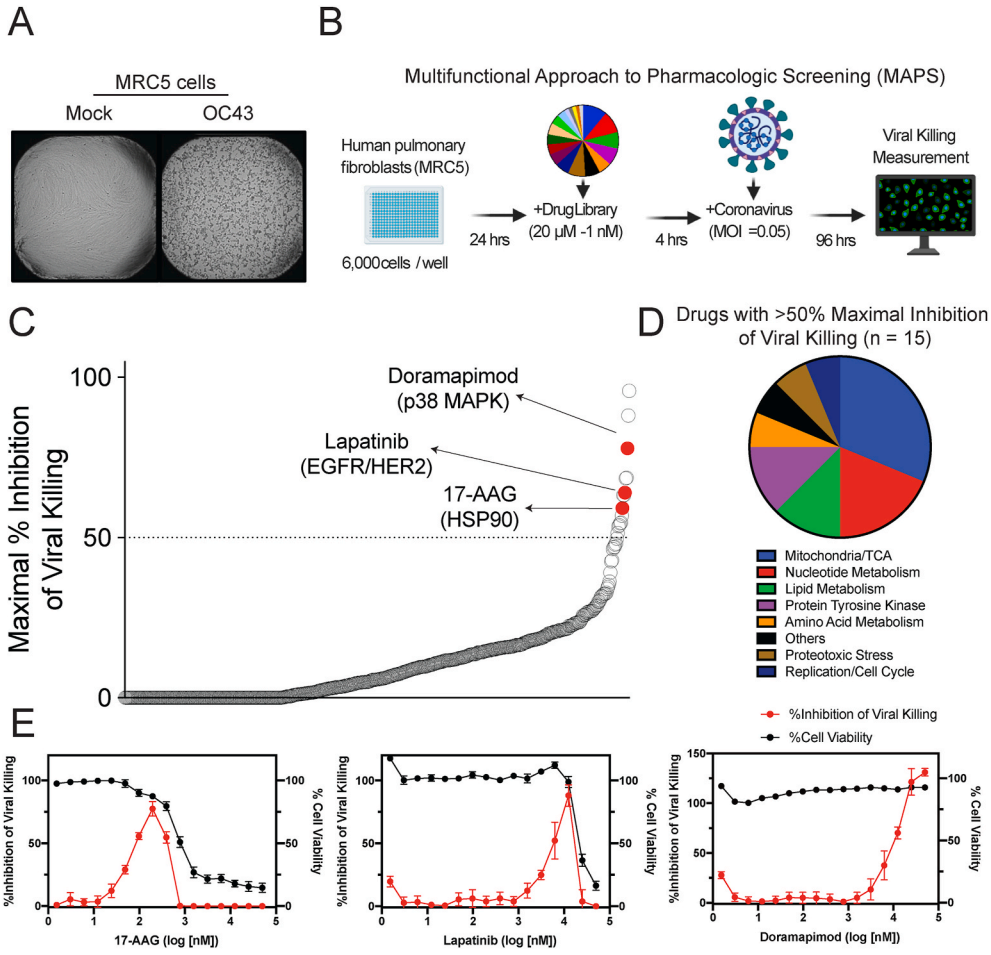

Fig. 1. Inhibitors of viral-induced killing identified using high-throughput screening. **(A)** MRC5 cells were infected with OC43 at an MOI of 0.05. Representative images of MRC5 96 h post infection. **(B)** Schematic of the Multifunctional Approach to Pharmacologic Screening platform used to detect compounds that inhibit coronavirus viral killing. Fibroblasts are seeded on a 384-well plate, incubated for 24 h, treated with the drug library and then infected with coronavirus. The ability of the compounds to inhibit viral killing is measured 96 h after infection by imaging the wells and counting nuclei. **(C)** Ranking of library compounds according to the maximal percent inhibition of viral killing across all concentrations. Data shown as mean, n = 2 **(D)** Pathways associated with the 15 compounds observed to inhibit viral killing by at least 50%. **(E)** Cell viability (black) and % inhibition of viral killing (red) is plotted against drug concentration for the top hits, 17-AAG, lapatinib and doramapimod. Data shown as mean ± SD, n = 6. See also Figs. S1 and S2, Table S1, and Table S2.

ability to detect any rescue from viral killing due to inherent cellular toxicity (Table S2). These findings illustrate the power of the MAPS platform, which identified hits that would have been most likely missed if the screen was performed at a single high drug concentration.

2.2. Hit compounds block coronavirus replication and synergize with remdesivir

Hit compounds were identified through high-throughput MAPS screening using reduction of CPE as a readout for viral inhibition. The antiviral activity of identified compounds was further validated by measuring the production of viral RNA and the cells' ability to produce infectious virus (TCID50). A dose-dependent reduction in viral RNA accumulation and TCID50 was observed across all drugs (Fig. 2A–B). Interestingly, 17-AAG was able to dramatically block viral RNA accumulation at doses almost 10-fold less than remdesivir, an antiviral with potent activity against SARS-CoV-2 in vitro. Next, we investigated whether our hit compounds could be combined with remdesivir to synergistically block CPE. While remdesivir can block SARS-CoV-2 in vitro, recent clinical trials have shown it not to be effective in patients (Pan et al., 2020). One potential limitation of remdesivir treatment is that its IC50 against SARS-CoV-2 is in the μM range, and plasma concentrations in COVID-19 infected patients treated with remdesivir are sub-μM (Tempestilli et al., 2020). Indeed, the IC50 of remdesivir against OC43-induced CPE was in the μM range (Fig. 2C–D). Importantly, co-treatment with either lapatinib or doramapimod reduced the IC50 of remdesivir into the sub-μM range (Fig. 2C–D, Figs. S3A–B). In addition, lapatinib and doramapimod worked synergistically with remdesivir to attenuate OC43-induced cell death at specific concentrations, e.g., ~2–5 μM for lapatinib, and ~10–20 μM for doramapimod (Figs. S3A–B). These results suggest that in addition to blocking OC43 betacoronavirus activity on their own, these compounds could potentially be combined with remdesivir to more effectively limit SARS-CoV-2 replication.

2.3. MRC5-ACE2 cells are an effective model of SARS-CoV-2 infection

The betacoronavirus OC43 was used as a surrogate of SARS-CoV-2 for high-throughput screening purposes because it can be safely handled under BSL2 containment (unlike SARS-CoV-2). While our hit compounds displayed impressive antiviral action against OC43, the ultimate goal was to identify potential therapeutics for SARS-CoV-2 infection. Expression of ACE2 is required for entry of SARS-CoV-2, and overexpression of ACE2 in cells has been effective at permitting infection, although this has largely been examined in transformed cancer cell lines (Dittmar et al., 2021), which could potentially confound findings. Instead, we decided to express ACE2 in MRC5 cells to create MRC5-ACE2 cells (Fig. 3A). MRC5-ACE2 cells demonstrated robust SARS-CoV-2 infection, as indicated by elevated accumulation of viral RNA, which was comparable to Vero-E6 cells, especially at 24 h post infection (hpi) (Fig. 3B). Further, MRC5-ACE2 cells showed CPE after infection with SARS-CoV-2 at multiple multiplicities of infection (MOI) (Fig. 3C). As MRC5-ACE2 cells are of the appropriate species (human), genetic background (non-transformed), and tissue type (pulmonary), this model represents an important tool for SARS-CoV-2 research.

2.4. Lapatinib blocks SARS-CoV-2 infection alone or in combination with remdesivir

The hit compounds derived from our MAPS screen with OC43 were lapatinib, doramapimod, and 17-AAG. Since lapatinib and 17-AAG had the most antiviral activity against OC43, these compounds were tested against SARS-CoV-2. Lapatinib effectively blocked SARS-CoV-2 infection, as measured by the dramatic reduction in viral RNA accumulation (Fig. 4A). Interestingly, 17-AAG, which was the top hit against OC43, only minimally reduced SARS-CoV-2 RNA accumulation. There are potentially multiple reasons for the lack of effectiveness observed for 17-AAG against SARS-CoV-2 (dose, timing, differences between betacoronaviruses). Based on the differences in effectiveness of 17-AAG between OC43 and SARS-CoV-2, we decided to examine doramapimod, although it was less effective at blocking OC43 RNA accumulation and infectious virion production. Intriguingly, doramapimod was able to block SARS-CoV-2 RNA accumulation at a low μM concentration, although it was still not as inhibitory as lapatinib or remdesivir (Fig. 4B). Nonetheless, lapatinib and doramapimod also blocked SARS-CoV-2-induced CPE (Fig. 4C) and completely prevented SARS-CoV-2 N protein accumulation (Fig. 4D). The compounds did not induce any cellular toxicity to MRC5-ACE2 cells at the drug concentrations tested (Fig. S4). Finally, our hit compounds were combined with remdesivir to examine whether these compounds could be combined to synergistically block SARS-CoV-2 infection. Both lapatinib and doramapimod were able to dramatically reduce the dose of remdesivir required to abolish SARS-CoV-2 RNA accumulation and production of infectious virions (Fig. 4E). Further, no toxicity was observed upon treatment with these compounds in combination with remdesivir (Fig. S5). These findings suggest that our top hit compounds lapatinib and doramapimod are potentially effective therapeutic options for patients infected with SARS-CoV-2 and can be used synergistically with remdesivir to lower its effective concentration.

3. Discussion

Our pharmacological screen identified several compounds capable of blocking the in vitro replication of two betacoronaviruses. We screened against OC43, which is a common human coronavirus that typically causes mild to moderate upper respiratory tract infections. Hit compounds were subsequently found to inhibit SARS-CoV-2, which is responsible for the COVID-19 pandemic and over 1 million deaths globally. Of particular interest was the finding that lapatinib could inhibit SARS-CoV-2 RNA replication in pulmonary fibroblasts by over 50,000-fold (Fig. 4B). Lapatinib is an FDA-approved compound with a favorable toxicity profile in patients (Baselga et al., 2012). Further, lapatinib concentrations found to inhibit SARS-CoV-2 are readily achievable in human tissues at currently prescribed doses (Spector et al., 2015). These results suggest that lapatinib could be an effective therapeutic to attenuate SARS-CoV-2 associated morbidity and mortality that could be quickly transitioned to the clinic. The need for effective therapeutics to treat SARS-CoV-2 is immense given its devastating effect on global human health, as well the recent disappointing results from the SOLIDARITY trial indicating that other potential antivirals such as remdesivir and hydroxychloroquine are not clinically effective (Pan et al., 2020).

Traditional drug screening libraries contain a wide range of compounds at a single high concentration dose. While useful for drug discovery with biochemical assays, these libraries are less suited for more complicated screens with live cells in which success depends on multiple parameters that can be affected by drug concentration, e.g. those affecting viral replication or cellular enzymes important for viability. Our current screen examined compounds across a wide range of doses (20 μM to 1 nM), which enabled us to identify concentrations of compounds that inhibit virally-induced killing, as well as those concentrations that contribute to toxicity during mock infection – allowing us to identify a preclinical therapeutic window. Further, traditional screening at a single high dose will miss compounds that are effective antivirals at lower concentrations, but toxic at higher concentrations, i.e., single dose screening increases false negatives. Finally, dose-response screening enables assessment of how partial inhibition of essential activities might impact viral infection, which is a significant limitation of most genetic screening studies (Birsoy et al., 2015; Shalem et al., 2014).

Our results indicate that the hit compounds identified via screening against a minimally pathogenic BSL2 coronavirus can identify compounds that inhibit the more pathogenic SARS-CoV-2 virus, a BSL3 agent. This has significant implications for antiviral development more

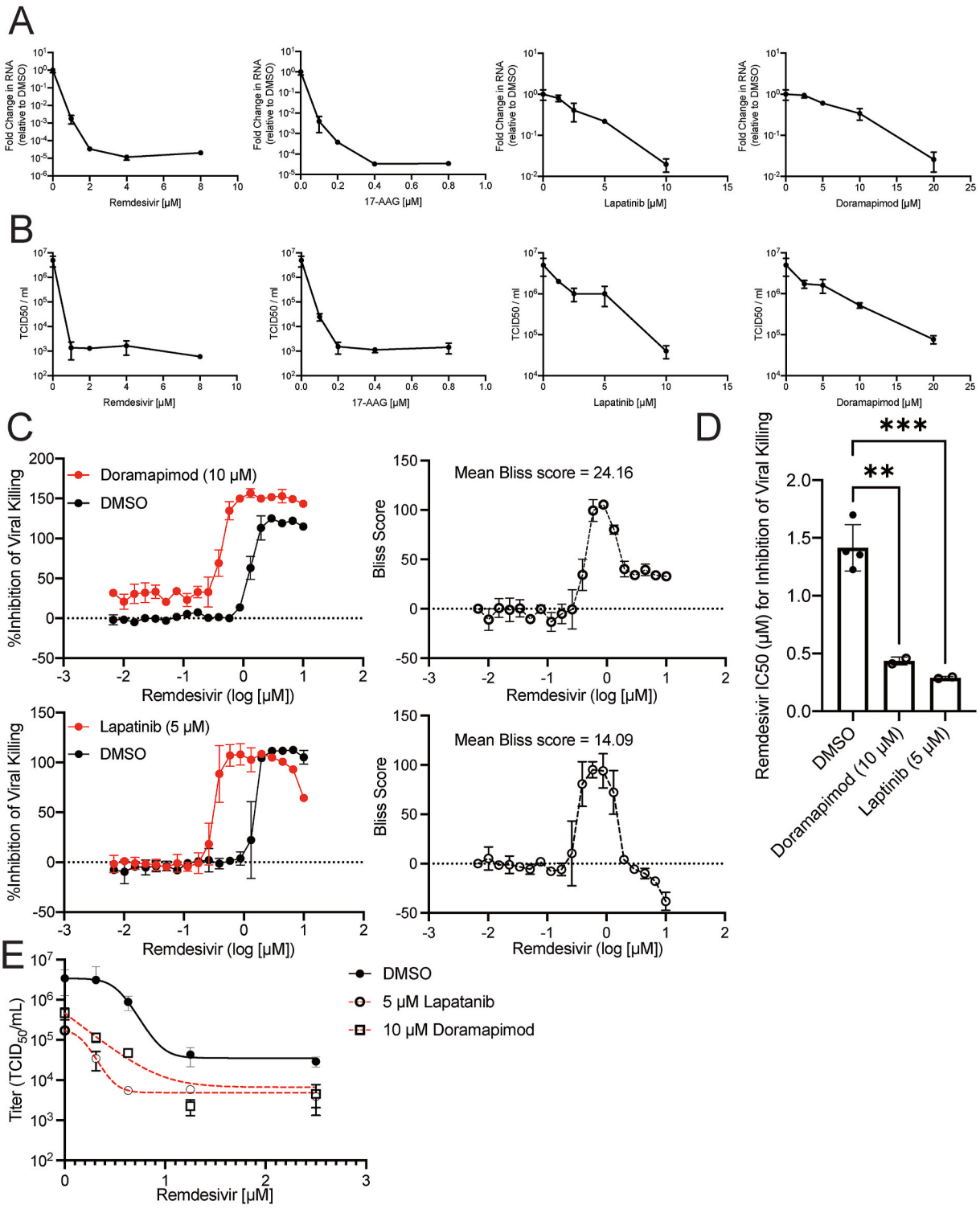

Fig. 2. Hit compounds inhibit OC43 replication and synergize with remdesivir.
(A–B) Confluent MRC5 cells were pretreated with DMSO (0.25%), remdesivir, 17-AAG, lapatinib, or doramapimod at the indicated concentrations for 3 h. After pretreatment, cells were infected with OC43 at an MOI of 0.05 in the presence of the appropriate drug concentration. At 24 hpi, RNA **(A)** and virus containing supernatants **(B)** were harvested. cDNA was synthesized from the RNA, and relative OC43 RNA levels were quantified. RNA levels were normalized to levels from DMSO treated samples **(A).** Data are from n = 3 biological replicates represented as mean ± SD. The virus containing supernatants were titered by TCID50 **(B).** Data are from n = 3 biological replicates represented as mean ± SD. **(C)** Percent inhibition of viral killing was plotted against remdesivir drug concentration either alone (black curve) or in combination with 10 μM doramapimod (red curve) (top) or 5 μM lapatinib (red curve)(bottom) and Bliss synergy scores were calculated for each drug combination (right). Data shown as mean ± SD, n = 2. **(D)** IC50 values from **(C).** Data are from n = 2 biological replicates represented as mean ± SD. $^{**}P<0.01$, $^{***}P<0.001$. Dunnett's multiple comparisons test was used to determine statistical significance for **(D).** **(E)** Viruses were titered by TCID50 for each combination of remdesivir with either 10 μM doramapimod or 5 μM lapatinib. Data are from n = 3 biological replicates represented as mean ± SD.

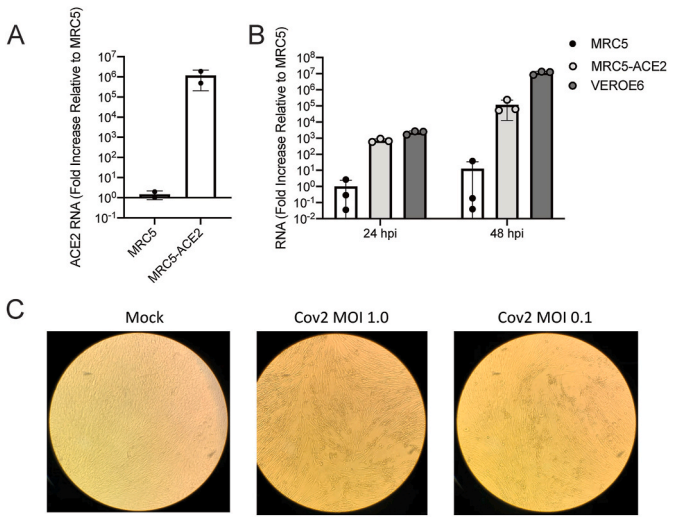

Fig. 3. SARS-CoV-2 replicates in MRC5 cells expressing ACE2. (A) Confluent MRC5 cells and MRC5 cells expressing ACE2 (MRC5-ACE2) were harvested, and their RNA isolated prior to synthesizing their cDNA. Relative SARS-CoV-2 RNA levels were quantified and normalized to the levels in MRC5 cells. Data are from n = 3 biological replicates represented as mean ± SD. **(B)** Confluent Vero-E6, MRC5, and MRC5-ACE2 cells were infected with SARS-CoV-2 at an MOI of 0.01. At 24 and 48 hpi, RNA was harvested and cDNA was synthesized. Relative SARS-CoV-2 RNA levels were quantified and normalized to the levels in MRC5 cells. Data are from n = 3 biological replicates represented as mean ± SD. **(C)** Representative images of MRC5-ACE2 cells either mock infected or infected with SARS-CoV-2 at an MOI of 1.0 or 0.1 at 96 hpi.

broadly. Specifically, high-throughput screening at BSL3 or BSL4 conditions is a major impediment to the ability to conduct antiviral screening and thus represents a major barrier to the development of antiviral compounds that could block the most pathogenic viruses. The ability to screen against related BSL2 agents to identify promising compounds could spur the development of compounds against extremely pathogenic agents that require the strictest biocontainment levels.

Many pharmacological screens for SARS-CoV-2 inhibitors have been performed in Vero cells (Bojkova et al., 2020; Gordon et al., 2020), which are monkey kidney cells. Vero cells have many benefits as they are easy to culture, grow quickly, and grow SARS-CoV-2 to high titers, which has been an issue for many human cell lines due to the lack of expression of the SARS-CoV-2 receptor, ACE2. However, screening for antiviral compounds in Vero cells also has limitations. They are derived from an African green monkey (*Cercopithecus aethiops*), from a non-respiratory tissue, i.e., the kidney, and are capable of forming tumors. All of these factors can significantly impact both the cellular and the viral responses to compound treatment. Consistent with this, it has recently been found that many compounds capable of limiting SARS-CoV-2 in Vero cells, such as hydroxychloroquine, are ineffective in human lung epithelial cell lines (Dittmar et al., 2021). We, therefore, set out to develop a model using human, non-transformed, pulmonary cells. MRC5 cells fulfill these requirements, and after transduction with ACE2 are capable of robust SARS-CoV-2 infection (Fig. 3). We found MRC5 cells to be extremely amenable to high-throughput screening, and given their physiological relevance, i.e., human and non-transformed, they provide a robust platform for future antiviral screening.

While we find that lapatinib attenuates SARS-CoV-2 infection, the mechanisms through which it does so are less clear. Lapatinib is an EGFR/HER2 inhibitor used to treat HER2-positive breast cancer (Burris et al., 2005; Dhillon and Wagstaff, 2007). It is possible that SARS-COV-2 depends on EGFR/HER2 activity or a closely related protein kinase. If such is the case, we might have expected to identify other EGFR-related kinase inhibitors in our screen, e.g., gefitinib and erlotinib. These compounds were not identified, although we cannot rule significant differences in the kinase specificities of the various inhibitors in our library. Another possibility is that lapatinib is inhibiting an alternative target from the one it was designed to block. An in silico molecular docking study identified lapatinib as a putative inhibitor of the SARS-CoV-2 protease, 3CLpro (Ghahremanpour et al., 2020), which is important for productive SARS-CoV-2 infection, and a target for anti-coronaviral therapeutic development (De Clercq, 2006). However, despite these computational predictions, experimental results reported in the same publication suggested that lapatinib did not inhibit 3CLpro (Ghahremanpour et al., 2020). In contrast, a separate manuscript in pre-print suggests that lapatinib could, in fact, inhibit the activity of 3CLpro (Drayman et al., 2020). Regardless of the exact antiviral mechanism, given the immediate need for clinical therapeutics to treat SARS-CoV-2, lapatinib is a good candidate for rapid assessment in COVID-19 patients. Lapatinib is orally bioavailable, and has been found to accumulate in the plasma of human patients at ~1–3 μM concentrations, and achieve ~8–12 μM concentrations in tissue samples (Spector et al., 2015). We observe significant inhibition at these concentrations *in vitro* suggesting that lapatinib could be effective at concentrations that occur in human patients. Further, lapatinib is well tolerated in patients with mostly mild adverse effects (Dhillon and Wagstaff, 2007). Collectively, the pharmacokinetic and safety profiles of lapatinib suggest that it could be relatively quickly evaluated in the clinic with respect to its ability to attenuate SARS-CoV-2-associated morbidity.

With respect to treatment of SARS-CoV-2, remdesivir, although very effective in vitro, has not been effective in patients (Pan et al., 2020) for uncertain reasons. Remdesivir is a pro-drug, that gets transformed into a bioactive nucleoside monophosphate derivative, GS-441524, which targets viral RNA-dependent RNA polymerases. Previous studies have shown that remdesivir can maximally accumulate to approximately 4–9 μM in plasma of healthy patients, while GS-441524 maximally accumulates to concentrations of about 0.5 μM (Jorgensen et al., 2020). In vitro, remdesivir exhibited an EC50 between 0.6 and 1.5 μM, and GS-441524 demonstrated an EC50 between 0.5 and 1.1 μM, with different activities in different cell types as a potential explanation for the range of values (Pruijssers et al., 2020). These data suggest that while remdesivir could inhibit SARS-CoV-2 replication at achievable plasma concentrations, the accumulation of its active derivative GS-441524 is likely sub-optimal for its antiviral activity. Further, in remdesivir treated COVID-19 patients, remdesivir was not detectable in bronchoalveolar aspirates, and GS-441524 was only detected at ~15 nM concentrations (Pan et al., 2020), significantly below the EC50. These data suggest that the availability of these compounds to the lung may limit their effectiveness in COVID-19 patients, which could be responsible for their lack of clinical efficacy (Pan et al., 2020). Combinations of antiviral compounds have been very successful clinically in limiting viral pathogenesis, e.g., with HIV-1. Here, we find that both lapatinib and doramapimod are capable of acting synergistically with remdesivir to attenuate SARS-CoV-2 replication, i.e., reducing the concentrations required for their antiviral activity. These results raise the possibility that treatment with lapatinib or doramapimod in combination with remdesivir could substantially improve clinical efficacy. While additional investigations are required, including *in vivo* validation of drug efficacies, our findings point to novel SARS-CoV-2 treatment options for patients, and potentially improved outcomes during this unprecedented pandemic.

4. Limitations of the study

There are two main limitations of this study. First, it is unclear the extent to which lapatinib would prevent SARS-CoV-2 infection *in vivo*. Efficacy data in animal models would encourage confidence in the pursuit of lapatinib as a potential anti-SARS-CoV-2 therapeutic. This work would benefit from the continued development of animal models that faithfully recapitulate SARS-CoV-2-associated replication and

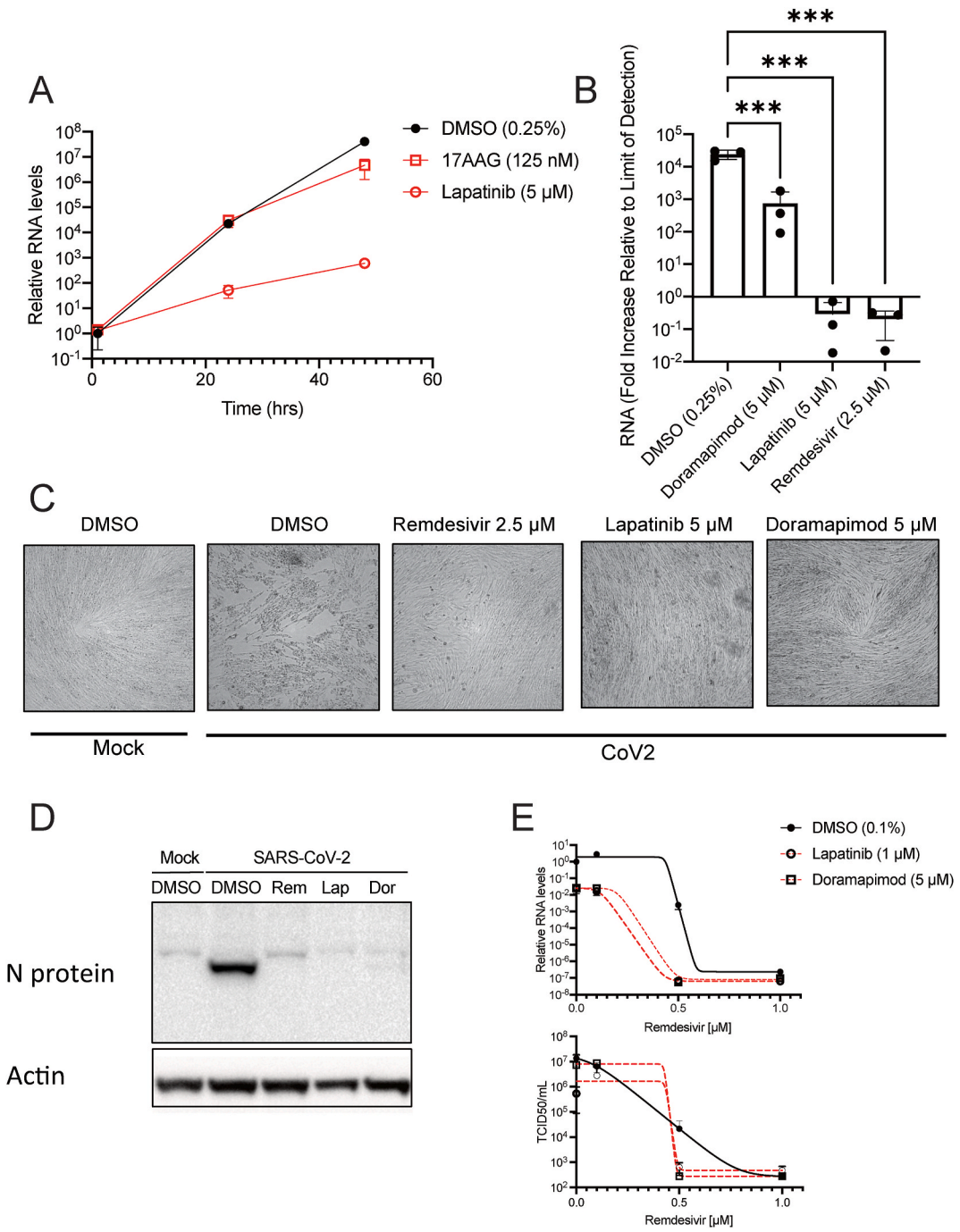

Fig. 4. Lapatinib and doramapimod inhibit SARS-CoV-2 replication alone or in combination with remdesivir. (A) Confluent MRC5-ACE2 cells were pre-treated with DMSO, 17-AAG, or lapatinib at the indicated concentrations for 4 h. After pretreatment, cells were infected with SARS-CoV-2 at an MOI of 0.01 in the presence of the appropriate drug. At 1, 24, and 48 hpi, RNA was harvested and cDNA was synthesized. Relative SARS-CoV-2 RNA levels were quantified and normalized to levels of the DMSO treated sample at 1 hpi. Data are from two biological replicates represented as mean ± SD. **(B–C)** Confluent MRC5-ACE2 cells were pretreated with DMSO, doramapimod, remdesivir, or lapatinib at the indicated concentrations for 4 h. After pretreatment, cells were infected with SARS-CoV-2 at an MOI of 0.01 in the presence of the appropriate drug. At 1 and 48 hpi, RNA was harvested and cDNA was synthesized. **(B)** Relative SARS-CoV-2 RNA levels at 48 hpi were quantified, and normalized to levels of the DMSO treated sample at 1 hpi. Data are from n = 3 biological replicates represented as mean ± SD. **(C)** At 48 hpi, cells were fixed, and imaged to examine cytopathic effect. **(D)** Immunoblot analysis of MRC5-ACE2 cells infected with mock or SARS-CoV-2 (MOI = 1) and pretreated with either remdesivir (Rem, 2.5 μM), lapatinib (Lap, 5 μM) or doramapimod (Dor, 5 μM). Cells were harvested at 24 hpi. **(E)** Confluent MRC5-ACE2 cells were pretreated with remdesivir at the indicated concentrations along with DMSO, lapatinib or doramapimod, infected with SARS-CoV-2 at an MOI of 0.01 in the presence of the appropriate drug. At 48 hpi, viral supernatant or RNA was harvested and cDNA was synthesized. Relative SARS-CoV-2 RNA levels were quantified and normalized to levels of the DMSO treated sample (top). Data are from n = 3 biological replicates represented as mean ± SD. ***P<0.001. Dunnett's multiple comparisons test was used to determine statistical significance for **(B)**. Virus containing supernatants were titered by TCID50 (bottom). See also Figs. S4 and S5.

pathology in people. A second major limitation is that the mechanisms through which lapatinib inhibits SARS-CoV-2 are unclear. Elucidating these mechanisms could provide avenues for additional or more specific therapeutic development. Despite these limitations, lapatinib is a prime candidate for further clinical evaluation, given that it is FDA approved and exhibits anti-SARS-CoV-2 activity at clinically achievable concentrations.

5. Materials and methods

5.1. Cell culture, viruses, and viral infection

Telomerase-immortalized MRC5 fibroblasts (MRC5 cells) were cultured in Dulbecco's modified Eagle serum (DMEM; Invitrogen) supplemented with 10% (vol/vol) fetal bovine serum (FBS) (Atlanta Biologicals), 4.5 g/L glucose, and 1% penicillin-streptomycin (Pen-Strep; Life Technologies) at 37 °C in a 5% (vol/vol) CO_2 atmosphere. Vero-E6 cells were cultured in Eagle's Minimum Essential Medium (ATCC, #30–2003) supplemented with 10% (vol/vol) fetal bovine serum (FBS) (Atlanta Biologicals), 4.5 g/L glucose, 1X Glutamax (Life Technologies, #35050061), and 1% penicillin-streptomycin (Pen-Strep; Life Technologies, #15140122) at 37 °C in a 5% (vol/vol) CO_2 atmosphere. Viral stocks of OC43 were propagated in MRC5 cells in 2% (vol/vol) FBS, 4.5 g/L glucose, and 1% penicillin-streptomycin at 34 °C. Viral stock titers were determined by TCID50 analysis in MRC5 cells. For the assessment of OC43 viral replication, viral titer was determined via TCID50 analysis in MRC5 cells. The SARS-CoV-2 isolate, Hong Kong/VM20001061/2020, was previously isolated from a nasopharyngeal aspirate and throat swab from an adult male patient in Hong Kong and was obtained through BEI resources (NR-52282). Viral stocks of SARS-CoV-2 were propagated in Vero-E6 cells in 2% (vol/vol) FBS, 4.5 g/L glucose, and 1% penicillin-streptomycin at 37 °C. Viral stock titers were determined by TCID50 analysis in Vero-E6 cells. All experiments involving live SARS-CoV-2 were conducted in a biosafety level 3 facility at the University of Rochester. ACE2-expressing MRC5 cells were generated via lentiviral transduction. For the generation of lentivirus, 293T cells (~50% confluent) were transfected with 2.6 μg pLenti-ACE2, 2.4 μg PAX2, and 0.25 μg vesicular stomatitis virus G glycoprotein using the Fugene 6 transfection reagent (Promega) according to the manufacturer's protocol. Twenty-four hours later, the medium was replaced with 5 ml of fresh medium. Lentivirus–containing medium was collected after an additional 24 h and filtered through a 0.45 μm pore-size filter prior to transduction. Telomerase-immortalized MRC5 fibroblasts were transduced with lentivirus in the presence of 5 μg/ml polybrene (Millipore Sigma) and incubated overnight. The lentivirus-containing medium was then removed and replaced with fresh medium. The cells were subsequently passaged in the presence of puromycin at 1 ug/ml and remained under selection for 3 days.

5.2. Compound library and high-throughput compound screening

The compound library for the high-throughput screen was prepared as described (Harris et al., 2019). Prior to screening with the compound library, the robustness of our screening method was determined by obtaining a Z' factor (Zhang et al., 1999). Each well of a 384-well pate (Corning, 3764) was seeded with 6000 MRC5 cells in a volume of 30 μL using a Multidrop Combi reagent dispenser (Thermo Scientific). Cells were then incubated at 37 °C for 24 h at which point cells were either given 20 μL of media for a mock infection or 20 μL media containing OC43 to achieve an MOI of 0.05 TCID50/mL. Cells were then incubated at 34 °C for 96 h whereupon the average and standard deviation of the number of cells was used to determine the Z' factor of 0.66. To determine compounds that inhibit the cytopathic effect observed with OC43 infection, 30 μL of MRC5 were seeded per well of 384-well plate and incubated at 37 °C. After 24 h, 100 nL of compounds from the library plates were pin transferred onto the cells and incubated at 34 °C for 4 h at which point 20 μL of media containing OC43 was added to infect the cells at an MOI of 0.05. The infected plates were then incubated at 34 °C for 96 h and cell numbers were quantified. Percent inhibition of viral killing was determined as: (Cell Number $Infected_{(Drug)}$ – Average Cell Number $Infected_{(DMSO)}$/(Average Cell Number Mock $Infection_{(DMSO)}$ – Average Cell Number $Infected_{(DMSO)}$)*100%. All values calculated to be negative were set to "0". Data post-processing was conducted using R and Prism scripts.

5.3. Quantification of Cell numbers

For cell culture experiments in 96-well (Greiner Bio-One, #655160) or 384-well (Corning, #3764) plate formats, cells were washed with PBS (Thermo Fisher, BP399-20), fixed using 4% formaldehyde (Sigma, #252549) and stained with 5 μg/mL Hoechst 33342 (Thermo Fisher). Cells were then imaged using a Cytation 5 imaging reader (BioTek). Each well was imaged using a 4X magnification objective lens and predefined DAPI channel with an excitation wavelength of 377 nm and emission wavelength of 447 nm or GFP channel with an excitation wavelength of 469 nm and emission wavelength of 525 nm Gen5 software (BioTek) was used to determine cell number by gating for objects with a minimum intensity of 3000, a size greater than 5 μm and smaller than 100 μm.

5.4. Drug synergy

To identify synergistic effects between the compounds identified in our screen and remdesivir, MRC5 were seeded in a 384-well plate as described for screening and incubated at 37 °C for 24 h. Using a D300 liquid dispenser (Hewlett-Packard), remdesivir was added following 1:2 dilution curve going down the rows of each plate starting at 10 μM in row C and ending at 0.01 μM in row N. Hit compounds were then added using a 19-point dose response curve across the columns with 1:1.5 dilution so that the concentration ranged from 20 μM in column 3 to 0.01 μM in column 21. After compounds were added to the cells, the plates were incubated at 34 °C for 4 h. Plates were then infected with OC43 at an MOI of 0.05 and incubated at 34 °C for 96 h at which point cell numbers were counted and inhibition of viral killing was calculated as indicated above. Bliss synergy scores for inhibition of viral killing were calculated using Synergy Finder 2.0 (Ianevski et al., 2020).

5.5. ACE2 cloning

The human angiotensin-converting enzyme 2 (hACE2) cDNA was amplified by PCR from the hACE2 plasmid (Addgene #1786) using the following primers:

1) 5'-CTT TAA AGG AAC CAA TTC AGT CGA CTG GAT CAT GTC AAG CTC TTC CTG GCT CCT TCT CAG-3'
2) 5'-ACC ACT TTG TAC AAG AAA GCT GGG TCT AGT TAA GCG GGC GCC ACC TGG GAG GTC TCG GTA-3′

PCR-amplified hACE2 cDNA was cloned via Gibson assembly into the BamHI and XbaI sites of pLenti CMV/TO-RasV12-puro backbone (Addgene #22262), to generate pLenti-ACE2.

5.6. Analysis of protein accumulation during SARS-CoV-2 infections and drug treatment

MRC5-ACE2 fibroblast were grown to confluence on a 6-well plate (Greiner Bio-One, #657160) and then pretreated with media containing either DMSO (0.25% vol/vol), lapatinib (5 μM), doramapimod (5 μM), or remdesivir (2.5 μM). After 4 h, cells were either mock infected or infected with SARS-CoV-2, Isolate Hong Kong/VM20001061/2020 (BEI Resources NR-52282) at an MOI of 0.01. After a 1-h adsorption period, viral inoculum was removed and replaced with media containing drug

or DMSO. Samples were harvested in SDS-lysis buffer at 4 and 24 h post infection. Protein lysates were treated with Laemmli SDS sample buffer (6X; Boston BioProducts, #BP-111R) with 5% β-mercaptoethanol for 10 min at 100 °C and then pelleted via centrifugation at 14,500 RPM for 5 min. Samples were run on 4–20% polyacrylamide gels (Genescript, #M42015) and transferred onto Immobilon-P PVDF membranes (MilliporeSigma, #ISEQ00010). Membranes were blocked with 5% milk in TBST for 1 h and blotted overnight with indicated antibodies in TBST with 0.05% bovine serum albumin (BSA). Excess primary antibodies were rinsed away with TBST and rinsed with secondary antibodies in TBST and 0.05% BSA for 1 h and rinsed again in TBST. Signal was visualized using Clarity Western ECL Substrate (Bio-Rad, #1705060). The following antibodies were used for immunoblot analysis: N-Protein Antibody (SinoBiological, #40068-RP02) and β-Actin (Sigma, #A1978).

5.7. Immunofluorescent staining of OC43 N-Protein

MRC5 cells were grown to confluence in a 96-well dish and infected with mock or OC43 at an MOI of 0.01 or 1. At 48 h post infection, cells were washed 3x with PBS and fixed with 2% paraformaldehyde in PBS for 15 min at room temperature. Cells were washed 3x with PBS and permeabilized with PBS containing 0.1% TritonX-100 for 15 min at room temperature. Cells were blocked with PBS containing 2% BSA and 0.05% Tween-20 for 1 h at room temperature. N-protein antibody (Sino Biological #40068) was prepared to 1:1000 dilution in PBS containing 0.5% Tween-20 and added to each well for 1 h. Cells were washed 3x with PBS containing 0.01% Tween-20. Secondary antibody (alexa flour 594 goat-anti-rabbit IgG, Invitrogen #a-11012) was prepared to 1:1000 in PBS containing 0.5% Tween-20 and added to each well for 1 h. Cells were washed 3x with PBS containing 0.05% Tween-20, Hoeschet stain (1:1000) was added to the final wash of PBS. Cells were imaged using the Cytation 5 imaging reader (BioTek). Each well was imaged using a 20X magnification objective lens with a predefined DAPI channel (described above) and predefined Texas Red channel with an excitation wavelength of 586 nm and emission wavelength of 603 nm.

5.8. Analysis of RNA

Before infection with OC43, MRC5 cells were grown to confluence in 12-well dishes. Cells were pretreated with 400 μl of medium containing drug or DMSO. After 3 h, 100 μl of inoculum containing the appropriate drug was added to each well at a multiplicity of infection (MOI) of 0.05. After a 1.5-h adsorption, 500 ul of media containing the appropriate drug was added to each well for a final volume of 1 mL/well. For infection with SARS-CoV-2, confluent MRC5 cells were pretreated with 400 μl of media or media containing drug or DMSO for 4 h. Media was then aspirated and replaced with 200 μl of inoculum containing the appropriated drug at an MOI of 0.01. After 1 h of adsorption, the inoculum was aspirated and replaced with 1 mL of media or media containing drug or DMSO. OC43 infections were cultured in media containing 10% FBS at 34 °C, while SARS-CoV-2 infections were cultured in media containing 2% FBS at 37 °C. At the indicated times RNA was isolated from infected cells via TRIzol (Invitrogen) extraction, according to the manufacturer's instructions and used to synthesize cDNA with the qScript cDNA Synthesis Kit (Quantabio). Relative quantities of gene expression were measured and normalized to GAPDH levels via the $2^{-\Delta\Delta CT}$ method using the following primers: OC43: 5'-GGATTGTCGCCGACTTCTTA-3' (forward) and 5'-CACACTTCTACGCCGAAACA-3' (reverse), SARS-CoV-2: 5'-ATGAGCTTAGTCCTGTTG-3' (forward) and 5'-CTCCCTTTGTTGTGTTGT-3' (reverse), and human GAPDH: 5'-CATGTTCGTCATGGGTGTGAACCA-3' (forward) and 5'-ATGGCATGGACTGTGGTCATGAGT-3'. For the analysis of ACE2 expression, total cellular RNA was extracted with TRIzol (Invitrogen) and used to generate cDNA using SuperScript II reverse transcriptase (Invitrogen) according to the manufacturer's instructions. Transcript abundance was measured by qPCR using Fast SYBR Green master mix (Applied Biosystems), a model 7500 Fast real-time PCR system (Applied Biosystems), and the Fast 7500 software (Applied Biosystems). Gene expression equivalent values were determined using the $2^{-\Delta\Delta Ct}$ method and normalized to GAPDH levels. Biological replicates were analyzed in technical duplicate. Outlier qPCR samples were identified via analysis of GAPDH Ct values that were beyond 1.5 times the interquartile range. For reactions in which the Ct value was undetermined, the limit of detection was set to either a Ct value of 40, or the amount of input inoculum (Ct value of ~37), if it was measured for a given experiment. The expression of hACE2 was confirmed by qPCR using the following primers:

forward primer 5′- GGA GTT GTG ATG GGA GTG ATA G -3′
reverse primer 5′- ATC GAT GGA GGC ATA AGG ATT T -3′

5.9. Drug toxicity

For toxicity of individual drugs, MRC5 and MRC5-ACE2 cells were grown to confluence in a 12-well dish in media containing 2% FBS at 37 °C. An eight-point 1:2 dilution scheme was made for each drug in media containing 2% FBS using 10 mM stock of drug that was stored in DMSO, starting with the following high concentrations: 17-AAG (1 μM), lapatinib (20 μM), remdesivir (20 μM), doramapimod (20 μM) alongside a 0.25% DMSO (v/v) control. At t0, wells were treated with 1 mL drug of each dilution (n = 3). One plate (n = 12) was fixed at t0 for a baseline cell count. At t = 48 hpt and t = 96 hpt drug-treated wells were fixed, stained and imaged. Media was aspirated from each well and wells were washed with 500 μl PBS then fixed and stained in 500 μl 4% paraformaldehyde/Hoechst (Invitrogen, #H3570) diluted 1:2000 in PBS for 30 min at room temperature. Cells were washed with PBS and nuclei were counted using Cytation 5 imaging software.

For toxicity of drugs acting synergistically, MRC5 and MRC5-ACE2 cells were grown to confluence in a 96-well dish in media containing 10% FBS at 37 °C. At t0, n = 30 wells for each cell type were stained with Hoechst and relative cell number was calculated for t0. Treatments were prepared in media containing 2% FBS and added to respective wells (n = 6 wells per treatment/timepoint). At t = 48 and t = 96 hpt drug-containing media was removed and replaced with PBS containing Hoechst stain diluted 1:2000 and Sytox Green (Invitrogen, #S7020) diluted 1:1000. Cells incubated for 30 min at 37 °C. Nuclei and dead cells were quantified using Cytation 5 imager DAPI and GFP channels, respectively, as described above. Relative cell count was calculated by dividing the nuclei count of each well each well by the average total nuclei count of DMSO treated MRC5 and MRC5-ACE2 cells at 48 and 96 hpt (n = 24). Percent cell killing was calculated for each well by dividing the number of dead cells quantified using Sytox Green by nuclei count.

5.10. Analysis of infectious virions by TCID50

To quantify drug treatment effects on infectious virion production, media was harvested from MRC5-ACE2 cells pretreated and infected with SARS-CoV2 (described above) and stored at -80 °C. Media samples were thawed and serially diluted 8X in MEM supplemented with 2% FBS. 50 μL each dilution was added to sub-confluent Vero-E6 cells which were in 50 μL MEM supplemented with 2% FBS (n = 12). After 1 day, 100 μL of MEM supplemented with 2% FBS was added to each well. Infected wells per dilution were counted 3 days post infection and used to calculate TCID50/mL.

6. Quantification and statistical analysis

6.1. Statistical analysis

All statistical analyses were completed using GraphPad Prism 9.0. Sigmoidal 4 point non-linear regression used for Figs. 2C, 4E, S4, and Table S2.

CRediT authorship contribution statement

M.H. Raymonda: initiated the study, Conceptualization, Methodology, interpreted the results, Writing – original draft, involved in conducting all experiments. **J.H. Ciesla:** initiated the study, Conceptualization, Methodology, interpreted the results, Writing – original draft, involved in conducting all experiments. **M. Monaghan:** initiated the study, Conceptualization, Methodology, interpreted the results, Writing – original draft, involved in conducting all experiments. **J. Leach:** assisted with OC43 experiments, assisted with BSL3 SARS-CoV-2 experiments. **G. Asantewaa:** assisted with BSL3 SARS-CoV-2 experiments. **L.A. Smorodintsev-Schiller:** assisted with high-throughput screening experiments. **M.M. Lutz:** IV: assisted with OC43 experiments. **X.L. Schafer:** cloned ACE2 vector, created MRC5-ACE2 cells. **T. Takimoto:** assisted with OC43 experiments. **S. Dewhurst:** assisted with BSL3 SARS-CoV-2 experiments. **J. Munger:** initiated the study, Conceptualization, Methodology, interpreted the results, Writing – original draft. **I.S. Harris:** initiated the study, Conceptualization, Methodology, interpreted the results, Writing – original draft.

Declaration of competing interest

The authors declare that they have no known competing financial interests or personal relationships that could have appeared to influence the work reported in this paper.

Acknowledgments

We would like to thank John Ashton and Tim Bushnell for their support regarding the frequent use of institutional high-throughput screening equipment. The following reagent was obtained through BEI Resources, NIAID, NIH: SARS-Related Coronavirus 2, Isolate Hong Kong/VM20001061/2020, NR-52282. The work was supported by NIH grants AI127370 and AI50698 to J.M, the American Association for Cancer Research and Breast Cancer Research Foundation (20-20-26-HARR) and Breast Cancer Coalition of Rochester to I.S.H and the T32 Training in HIV Replication and Pathogenesis (AI1049815) and Biochemistry/Molecular Biology (GM068411).

Appendix A. Supplementary data

Supplementary data to this article can be found online at https://doi.org/10.1016/j.virol.2021.11.008.

References

Baselga, J., Bradbury, I., Eidtmann, H., Di Cosimo, S., de Azambuja, E., Aura, C., Gómez, H., Dinh, P., Fauria, K., Van Dooren, V., et al., 2012. Lapatinib with trastuzumab for HER2-positive early breast cancer (NeoALTTO): a randomised, open-label, multicentre, phase 3 trial. Lancet 379, 633–640.

Birsoy, K., Wang, T., Chen, W.W., Freinkman, E., Abu-Remaileh, M., Sabatini, D.M., 2015. An essential role of the mitochondrial electron transport chain in cell proliferation is to enable aspartate Synthesis. Cell 162, 540–551.

Bojkova, D., Klann, K., Koch, B., Widera, M., Krause, D., Ciesek, S., Cinatl, J., Munch, C., 2020. Proteomics of SARS-CoV-2-infected host cells reveals therapy targets. Nature 583, 469–472.

Burris 3rd, H.A., Hurwitz, H.I., Dees, E.C., Dowlati, A., Blackwell, K.L., O'Neil, B., Marcom, P.K., Ellis, M.J., Overmoyer, B., Jones, S.F., et al., 2005. Phase I safety, pharmacokinetics, and clinical activity study of lapatinib (GW572016), a reversible dual inhibitor of epidermal growth factor receptor tyrosine kinases, in heavily pretreated patients with metastatic carcinomas. J. Clin. Oncol. 23, 5305–5313.

De Clercq, E., 2006. Potential antivirals and antiviral strategies against SARS coronavirus infections. Expert Rev. Anti-infect. Ther. 4, 291–302.

Dhillon, S., Wagstaff, A.J., 2007. Lapatinib. Drugs 67, 2101–2108 discussion 2109-2110.

Dittmar, M.L., Seung, Jae, Whig, Kanupriya, Segrist, Elisha, Li, Minghua, Jurado, Kellie, Samby, Kirandeep, Ramage, Holly, Schultz, David, Cherry, Sara, 2021. Drug repurposing screens reveal FDA approved drugs active against SARS-Cov-2. Cell Rep. 35 (1), 108959.

Drayman, N., Jones, K.A., Azizi, S.-A., Froggatt, H.M., Tan, K., Maltseva, N.I., Chen, S., Nicolaescu, V., Dvorkin, S., Furlong, K., et al., 2020. Drug repurposing screen identifies masitinib as a 3CLpro inhibitor that blocks replication of SARS-CoV-2 in vitro</em&gt. bioRxiv 2020 (2008), 2031.274639.

Ghahremanpour, M.M., Tirado-Rives, J., Deshmukh, M., Ippolito, J.A., Zhang, C.-H., Cabeza de Vaca, I., Liosi, M.-E., Anderson, K.S., Jorgensen, W.L., 2020. Identification of 14 known drugs as inhibitors of the main protease of SARS-CoV-2. ACS Med. Chem. Lett. 11 (12), 2526–2533.

Gordon, D.E., Jang, G.M., Bouhaddou, M., Xu, J., Obernier, K., White, K.M., O'Meara, M. J., Rezelj, V.V., Guo, J.Z., Swaney, D.L., et al., 2020. A SARS-CoV-2 protein interaction map reveals targets for drug repurposing. Nature 583, 459–468.

Harris, I.S., Endress, J.E., Coloff, J.L., Selfors, L.M., McBrayer, S.K., Rosenbluth, J.M., Takahashi, N., Dhakal, S., Koduri, V., Oser, M.G., et al., 2019. Deubiquitinases maintain protein homeostasis and survival of cancer cells upon glutathione depletion. Cell Metabol. 29 (5), 1166–1181.

Ianevski, A., Kiri, A.K., Aittokallio, T., 2020. SynergyFinder 2.0: visual analytics of multi-drug combination synergies. Nucleic Acids Res. 48, 488–493.

Jorgensen, S.C.J., Kebriaei, R., Dresser, L.D., 2020. Remdesivir: review of pharmacology, pre-clinical data, and emerging clinical experience for COVID-19. Pharmacotherapy 40, 659–671.

Kamal, A., Thao, L., Sensintaffar, J., Zhang, L., Boehm, M.F., Fritz, L.C., Burrows, F.J., 2003. A high-affinity conformation of Hsp90 confers tumour selectivity on Hsp90 inhibitors. Nature 425, 407–410.

Nicholson, H.E., Tariq, Z., Housden, B.E., Jennings, R.B., Stransky, L.A., Perrimon, N., Signoretti, S., Kaelin Jr., W.G., 2019. HIF-independent synthetic lethality between CDK4/6 inhibition and VHL loss across species. Sci. Signal. 12.

Pan, H., Peto, R., Karim, Q.A., Alejandria, M., Henao-Restrepo, A.M., García, C.H., Kieny, M.-P., Malekzadeh, R., Murthy, S., Preziosi, M.-P., et al., 2020. (2020). Repurposed antiviral drugs for COVID-19 –interim WHO SOLIDARITY trial results. medRxiv 2010, 2015.20209817.

Pargellis, C., Tong, L., Churchill, L., Cirillo, P.F., Gilmore, T., Graham, A.G., Grob, P.M., Hickey, E.R., Moss, N., Pav, S., et al., 2002. Inhibition of p38 MAP kinase by utilizing a novel allosteric binding site. Nat. Struct. Biol. 9, 268–272.

Pruijssers, A.J., George, A.S., Schäfer, A., Leist, S.R., Gralinksi, L.E., Dinnon, K.H., Yount, B.L., Agostini, M.L., Stevens, L.J., Chappell, J.D., et al., 2020. Remdesivir potently inhibits SARS-CoV-2 in human lung cells and chimeric SARS-CoV expressing the SARS-CoV-2 RNA polymerase in mice. Cell Rep. 32 (3), 107940.

Riva, L., Yuan, S., Yin, X., Martin-Sancho, L., Matsunaga, N., Pache, L., Burgstaller-Muehlbacher, S., De Jesus, P.D., Teriete, P., Hull, M.V., et al., 2020. Discovery of SARS-CoV-2 antiviral drugs through large-scale compound repurposing. Nature 586, 113–119.

Rodriguez-Sanchez, I., Schafer, X.L., Monaghan, M., Munger, J., 2019. The Human Cytomegalovirus UL38 protein drives mTOR-independent metabolic flux reprogramming by inhibiting TSC2. PLoS Pathog. 15, e1007569.

Shalem, O., Sanjana, N.E., Hartenian, E., Shi, X., Scott, D.A., Mikkelson, T., Heckl, D., Ebert, B.L., Root, D.E., Doench, J.G., et al., 2014. Genome-scale CRISPR-Cas9 knockout screening in human cells. Science 343, 84–87.

Shu, S., Wu, H.J., Ge, J.Y., Zeid, R., Harris, I.S., Jovanović, B., Murphy, K., Wang, B., Qiu, X., Endress, J.E., et al., 2020. Synthetic lethal and resistance interactions with BET bromodomain inhibitors in triple-negative breast cancer. Mol. Cell 78 (6), 1096–1113.

Spector, N.L., Robertson, F.C., Bacus, S., Blackwell, K., Smith, D.A., Glenn, K., Cartee, L., Harris, J., Kimbrough, C.L., Gittelman, M., et al., 2015. Lapatinib plasma and tumor concentrations and effects on HER receptor phosphorylation in tumor. PLoS One 10, e0142845.

Tempestilli, M., Caputi, P., Avataneo, V., Notari, S., Forini, O., Scorzolini, L., Marchioni, L., Ascoli Bartoli, T., Castilletti, C., Lalle, E., et al., 2020. Pharmacokinetics of remdesivir and GS-441524 in two critically ill patients who recovered from COVID-19. J. Antimicrob. Chemother. 75, 2977–2980.

Zhang, J.H., Chung, T.D., Oldenburg, K.R., 1999. A simple statistical parameter for use in evaluation and validation of high throughput screening assays. J. Biomol. Screen 4, 67–73.